1 **Supplemental Methods**

2 **Tissue microarray (TMA) construction.** For baseline WT and $Mtg16^{-/-}$ analyses, the TPSR

3 constructed 2 TMAs using the TMA Grand Master automated arrayer (PerkinElmer) from

4 individual FFPE blocks. Briefly, 2-mm cores were punched from FFPE blocks containing Swiss-

5 rolled WT and $Mtg16^{-/-}$ SI and colon (3 cores per Swiss roll). Following construction, H&Es were

6 generated from the TMAs and evaluated for quality before using the TMAs for IHC or other

7 staining.

8 **Bulk RNA-seq of human CRC and CAC samples.** RNA-seq of human samples collected from

9 9 regional hospitals in Finland was performed and analyzed as previously described (1). Briefly,

10 RNA was TRIzol-extracted from human tumor samples and underwent HiSeq LncRNA-Seq

11 library preparation and paired-end sequencing using Illumina HiSeqXTen. Raw sequences were

12 mapped onto the human transcriptome (Ensembl release 79) using Salmon (v0.12.0) (2). Gene-

13 level quantification with variance stabilization was performed using DESeq2 (v1.18.1) (3)

14 followed by limma (v3.34.9) correction of sequencing batch effects (4).

15 **AOM/DSS tumoroid cultures.** Colon tumors were isolated at sacrifice following the AOM/DSS

16 protocol. Tumoroids were generated as previously described (5). Briefly, tumors were diced and

17 incubated in 10 mL digestion buffer (0.1 mg/mL collagenase XI [#C7657, Sigma] and 0.125

18 mg/mL dispase II [#17105-041, Gibco] in complete Advanced DMEM [#12491015, Gibco]) at 37

19 °C on a nutating shaker for 2 h. Epithelial cells were mechanically dissociated by pipetting.

20 Supernatant containing the epithelial cells was centrifuged at 150 $x\ g$, 4 °C for 3 min, washed

21 twice in ice-cold PBS, and plated in 50-µL Matrigel (#356231, Corning) plugs overlaid with 500

22 µL MGM-CM (minigut media with R-spondin and Noggin conditioned media, generated as

23 previously described (5)) containing 0.002% primocin (#NC9141851, Invivogen). Tumoroids

24 were passaged by gentle dissociation to single cells in TrypLE (#12604013, Gibco) at 37 °C,

25 washing in ice-cold PBS, and replating at least once at approximately equivalent cell density to

26   remove debris and normalize the number of tumoroids/well before collecting them for analysis.

27   Tumoroid fixation and embedding in agarose for staining was then performed as previously

28   described (5).

29   **Protein isolation and immunoblotting.** Bone marrow was collected from the hindlegs of WT,

30    $Mtg16^{T/T}$, and $Mtg16^{-/-}$ mice as previously described (6). Pelleted bone marrow from each mouse

31   was resuspended in ACK Lysing Buffer (#A1049201, Gibco) for 2 min at RT and centrifuged at

32   300 $x\ g$, 4 °C for 30 s to lyse and remove red blood cells. Pellets were washed with ice-cold

33   PBS and incubated in 400 µL CelLytic MT Cell Lysis Reagent (#C3228, Sigma-Aldrich) with

34   gentle nutation for 15 min at 4 °C. Lysates were sonicated 10x with 1-s pulses and centrifuged

35   at 16,000 $x\ g$, 4 °C for 10 min to remove soluble material. Total protein concentration was

36   normalized using the Pierce BCA Assay Protein Assay Kit (#23225, Thermo Scientific). 100 µg

37   protein was removed from each lysate, combined with Laemmli buffer (final concentration 6.5%

38   β-mercaptoethanol), boiled at 95 °C for 5 min, and resolved using an 8% acrylamide/bis-

39   acrylamide gel containing 10% SDS (6% stack). Samples were transferred to a 0.2-µm Protran

40   Nitrocellulose Hybridization Transfer Membrane (#NBA083C001EA, PerkinElmer). The

41   membrane was rinsed in TBS to remove acrylamide residue, dried for 1 h at RT, rehydrated in

42   TBS at RT for 5 min, blocked at RT for 1 hour using Intercept TBS Blocking Buffer (#927-60001,

43   LI-COR), and incubated with 1:500 αMTG16 primary antibody (#17190-1-AP, Proteintech) in

44   antibody diluent (Intercept TBS Blocking Buffer with 0.2% Tween-20) overnight. The membrane

45   was then washed 3x in 0.2% TBS-T for 5 min and then incubated in 1:20,000 IRDye 800CW

46   Goat anti-Rabbit IgG Secondary Antibody (#926-32211, LI-COR) in antibody diluent for 1 h at

47   RT. The membrane was washed 3x in 0.2% TBS-T for 15 min, rinsed in TBS, and imaged using

48   the Odyssey CLx Infrared Imaging System (LI-COR) with LI-COR Image Studio.

49   **Data visualization and presentation.** Figures were generated using BioRender

50   (https://biorender.com/), GSEA (v4.1.0), the R packages Seurat (v4.0.4), pheatmap (v1.0.12),

51   RColorBrewer (v1.1-2), and ggplot2 (v3.2.1), Meta-Chart (https://www.meta-

52   chart.com/venn#/display), the Broad Institute Integrated Genomics Viewer (7) (v2.9.1),

53   GraphPad Prism (v9.0.1), the *Tabula Muris* (8) web interface (https://tabula-

54   muris.ds.czbiohub.org/), and Inkscape (v1.0.1).

55   **Code availability.** All code is available upon reasonable request.

56 **Supplemental Tables**

	Primary Antibody	Catalog #	Supplier	Species/ Isotype	Dilution	Antigen retrieval
Chromogenic IHC	α-SYP	ab32127	Abcam	Rabbit monoclonal [YE269]	1:800	Tris-EDTA pH 9.0 in a pressure cooker at 97 °C for 15 min followed by 10 min at RT
	α-DCLK1	62257	Cell Signaling Technologies (CST)	Rabbit monoclonal (IgG)	1:500	10 mM sodium citrate, pH 6.0 in a pressure cooker at 105 °C for 15 min followed by 10 min at RT
Immunofluorescent staining	α-E-cadherin	610182	BD Biosciences	Mouse monoclonal [36] (IgG$_{2a}$)	1:500	10 mM sodium citrate, pH 6.0 at 95 °C for 10 min followed by 30 min cooling at RT
	α-CHGA	20085	ImmunoStar	Rabbit polyclonal	1:2000	10 mM sodium citrate, pH 6.0 at 95 °C for 10 min followed by 30 min cooling at RT
	α-p-H3 (Ser 10)	06-570	Sigma-Aldrich	Rabbit polyclonal	1:400	10 mM sodium citrate, pH 6.0 at 95 °C for 10 min followed by 30 min cooling at RT
	α-CC3 (Asp175)	9661	CST	Rabbit polyclonal	1:400	10 mM sodium citrate, pH 6.0 at 95 °C for 10 min followed by 30 min cooling at RT
	α-γH2A.X (Ser139)	9718	CST	Rabbit monoclonal [20E3] (IgG)	1:400	10 mM sodium citrate, pH 6.0 at 95 °C for 10 min followed by 30 min cooling at RT
	α-Ly6B.2	MCA771G	Bio-Rad	Rat monoclonal (IgG$_{2a}$)	1:200	10 mM sodium citrate, pH 6.0 at 95 °C for 10 min followed by 30 min cooling at RT
	α-F4/80	MCA497G	Bio-Rad	Rat monoclonal [Cl:A3-1] (IgG$_{2b}$)	1:400	20 µg/mL proteinase K in TE buffer, pH 8.0 for 3 min at RT
	α-Ki67	Ab15580	Abcam	Rabbit polyclonal	1:500	10 mM sodium citrate, pH 6.0 at 95 °C for 10 min followed by 30 min cooling at RT

57 **Table S1. Antibodies and antigen retrieval used in chromogenic and immunofluorescent**
58 **staining.**

Category	Description	Score
Inflammation (0-3)	None	0
	Slight	1
	Moderate	2
	Severe	3
% involved by inflammation (1-4)	1-25%	1
	26-50%	2
	51-75%	3
	76-100%	4
Depth of inflammation (0-3)	None	0
	Mucosal	1
	Mucosal and submucosal	2
	Transmural	3
Crypt damage (1-4)	Basal 1/3 crypt cells damaged	1
	Basal 2/3 crypt cells damaged	2
	Only surface epithelium intact	3
	Entire crypt and epithelial surface lost	4
% involved by crypt damage (1-4)	1-25%	1
	26-50%	2
	51-75%	3
	76-100%	4
Epithelial regeneration (0-3)	Tissue appears normal (no residual injury/ complete epithelial regeneration)	0
	Slight epithelial injury with almost complete regeneration	1
	Surface epithelium not intact (regeneration present, but epithelial integrity has not been restored)	2
	Ulcer with no regeneration/tissue repair	3
Crypt distortion and branching (0-3)	Normal crypts	0
	Mild	1
	Moderate	2
	Severe (mucosa unable to regenerate normal crypt architecture)	3

Table S2. Histologic injury and regeneration scoring system. Adapted from Dieleman *et al*. (9) and Fukata *et al*. (10). Note that a higher epithelial regeneration score represents a decreased ability to regenerate.

Figure(s)	Gene set name	Description	Source
Differentiated epithelial cells (**Figs. 2B, 3F**)	Enteroendocrine (EE)	Expression signature defined for enteroendocrine cells following scRNA-seq and unbiased clustering of FACS-sorted murine intestinal epithelium	Haber *et al.* 2017 (11)
	L-cell	Genes enriched in L-cell cluster generated from droplet-based scRNA-seq of healthy human colon mucosa	Parikh *et al.* 2019 (12)
	Enterochromaffin	Genes enriched in enterochromaffin cluster generated from droplet-based scRNA-seq of healthy human colon mucosa	Parikh *et al.* 2019 (12)
	Absorptive	Expression signature defined for absorptive enterocytes following scRNA-seq and unbiased clustering of FACS-sorted murine intestinal epithelium	Haber *et al.* 2017 (11)
	Tuft	Expression signature defined for tuft cells following scRNA-seq and unbiased clustering of FACS-sorted murine intestinal epithelium	Haber *et al.* 2017 (11)
	Goblet	Expression signature defined for goblet cells following scRNA-seq and unbiased clustering of FACS-sorted murine intestinal epithelium	Haber *et al.* 2017 (11)
	BEST4/OTOP2+ colonocyte	Genes enriched in a novel BEST4/OTOP2+ colonocyte cluster generated from droplet-based scRNA-seq of healthy human colon mucosa	Parikh *et al.* 2019 (12)
Enteroendocrine (EE) progenitor cells (**Figs. 2B, 3F**)	Early EE	Genes enriched in FACS-sorted early EE progenitors identified using a novel "Neuorg3Chrono" pulse-chase reporter mouse that allows temporal resolution of cells in the EE lineage	Gehart *et al.* 2019 (13)
	Early/Intermediate EE	Genes enriched in FACS-sorted early and intermediate EE progenitors identified using a novel "Neuorg3Chrono" pulse-chase reporter mouse that allows temporal resolution of cells in the EE lineage	Gehart *et al.* 2019 (13)
	Intermediate EE	Genes enriched in FACS-sorted intermediate EE progenitors identified using a novel "Neuorg3Chrono" pulse-chase reporter mouse that allows temporal resolution of cells in the EE lineage	Gehart *et al.* 2019 (13)
	Intermediate/Late EE	Genes enriched in FACS-sorted intermediate and late EE progenitors identified using a novel "Neuorg3Chrono" pulse-chase reporter mouse that allows temporal resolution of cells in the EE lineage	Gehart *et al.* 2019 (13)
	Late EE	Genes enriched in FACS-sorted late EE progenitors identified using a novel "Neuorg3Chrono" pulse-chase reporter mouse that allows temporal resolution of cells in the EE lineage	Gehart *et al.* 2019 (13)
	Neurog3-EGFP+/+	Genes enriched in FACS-sorted *Neurog3*-EGFP+ intestinal epithelial cells from mice homozygous for the *Neurog3*-EGFP reporter	Li *et al.* 2020 (14)

Stem cells and progenitor cells (**Figs. 2C, 3G**)	*Bmi1*-GFP[+]	Genes enriched in FACS-sorted *Bmi1*-GFP[+] murine intestinal epithelial cells	Yan *et al.* 2017 (15)
	mTert-GFP[+]	Genes enriched in FACS-sorted *mTert*-GFP[+] murine intestinal epithelial cells	Yan *et al.* 2017 (15)
	FVR[Low]	Genes enriched in FACS-sorted *Fltp*-H2B-Venus reporter (FVR)[Low] murine intestinal epithelial cells. FVR[Low] cells were characterized as quiescent, terminally differentiated EE cells that had previously induced *Fltp* expression (activation of the WNT-PCP pathway).	Bottcher *et al.* 2021 (16)
	Rbpj-DBZ Sec-Pro	Genes enriched in intestinal crypts from both *Rbpj*^{-/-} and dibenzazepine(DBZ)-treated mice (2 independent ways of inhibiting Notch signaling to increase secretory progenitors [Sec-Pro])	Kim *et al.* 2014 (17)
	CD166[Hi]	Genes enriched in FACS-sorted CD166[Hi] (antibody-based) murine intestinal epithelial cells	Yan *et al.* 2017 (15)
	MKI67[Hi] ("GAO_LARGE_INTESTINE_ADULT_CH_MKI67HIGH_CELLS" in the MSigDB)	Genes enriched in *MKI67*[Hi] cell cluster from scRNA-seq of human colon from healthy adults	Gao *et al.* 2018 (18); available in the MSigDB (19)
	LRIG1[+]	Genes enriched in FACS-sorted LRIG1^{+} (antibody-based) murine intestinal epithelial cells	Powell *et al.* 2012 (20)
	Lgr5[+] ISC	See "Munoz2012_Lgr5-GFPHigh_ISC" (*Lgr5*^{+} stem cell gene sets).	Muñoz *et al.* 2012 (21)
	Lgr5[+] ISC (colon)	See "Murata2020_Lgr5_Stem-Cell_Colon_High" (*Lgr5*^{+} stem cell gene sets).	Murata *et al.* 2020 (22)
Lgr5[+] stem cell gene sets (**Fig. S6A**)	Yan2017-ISC-Lgr5-Cre_Pos_UP	Genes enriched in FACS-sorted *Lgr5*-eGFP[+] murine intestinal epithelial cells	Yan *et al.* 2017 (15)
	Basak2017_UP-in-active-cycling-Lgr5_Pos	Genes enriched in FACS-sorted *Lgr5*-eGFP[+] *Ki67*-RFP[+] murine intestinal epithelial cells	Basak *et al.* 2017 (23); derived from Basak *et al.* 2014 (24)
	Basak2017_UP-in-quiescent-Lgr5_Pos	Genes enriched in FACS-sorted *Lgr5*-eGFP[+] *Ki67*-RFP[-] murine intestinal epithelial cells	Basak *et al.* 2017 (23); derived from Basak *et al.* 2014 (24)

|			
	Munoz2012_Lgr5-GFPHigh_ISC	ISC signature derived from complementary transcriptomic (using multiple microarray platforms) and proteomic profiling of FACS-sorted *Lgr5*-eGFP^Hi cells. <u>This gene set was chosen for the main figures (**Figure 2C, 3G**) because it is widely used in the literature to represent *Lgr5*+ ISCs.</u>	Muñoz *et al.* 2012 (21)
	Murata2020_Lgr5_Stem-Cell_Colon_Total	Out of the genes specific to *Lgr5*+ ISCs according to Muñoz *et al.*(21), genes expressed at any level (> 1 RPKM) in FACS-sorted *Lgr5*$^{Dtr-GFP}$ cells from uninjured murine colon (401 genes)	Murata *et al.* 2020 (22)
	Murata2020_Lgr5_Stem-Cell_Colon_High	Out of the genes specific to *Lgr5*+ ISCs according to Muñoz *et al.*(21), genes expressed at "appreciable levels" (> 10 RPKM) in FACS-sorted *Lgr5*$^{Dtr-GFP}$ cells from uninjured murine colon (176 genes). <u>This gene set was chosen for the main figures (**Figure 2C, 3G**) because it was generated recently using colonic *Lgr5*+ stem cells.</u>	Murata *et al.* 2020 (22)
	Yan2017-SIclusters_C1_non-cycling-Lgr5-GFP	Genes enriched in cluster representing non-cycling *Lgr5*+ ISCs following scRNA-seq of FACS-isolated *Lgr5*-eGFP+ cells, *Bmi1*-GFP+ cells, and *Prox1*-GFP+ cells versus a fourth control sample of *Lgr5*-eGFP- intestinal epithelial cells	Yan *et al.* 2017 (15)
	GAO_LARGE_INTESTINE_24W_C5_LGR5POS_STEM_CELL	Genes enriched in *Lgr5*+ stem cell cluster from scRNA-seq of human fetal large intestine	Gao *et al.* 2018 (18); available in the MSigDB (19)
Intestinal epithelial signaling pathways (**Fig. S6B**)	GO_CANONICAL_WNT_SIGNALING_PATHWAY		MSigDB (19) (Gene Ontology [GO])
	GO_EPIDERMAL_GROWTH_FACTOR_RECEPTOR_SIGNALING_PATHWAY		MSigDB (19) (GO)
	GO_HIPPO_SIGNALING		MSigDB (19) (GO)
	GO_NON_CANONICAL_WNT_SIGNALING_PATHWAY		MSigDB (19) (GO)
	GO_NOTCH_SIGNALING_PATHWAY		MSigDB (19) (GO)
	HALLMARK_KRAS_SIGNALING_UP		MSigDB (19) (Hallmarks)
	KEGG_HEDGEHOG_SIGNALING_PATHWAY		MSigDB (19) (Kyoto Encyclopedia of Genes and Genomes [KEGG])
	KEGG_MAPK_SIGNALING_PATHWAY		MSigDB (19) (KEGG)
	KEGG_TGF_BETA_SIGNALING_PATHWAY		MSigDB (19) (KEGG)

|			
	PID_BMP_PATHWAY		MSigDB (19) (Protein Interactions Database [PID])
	PID_NOTCH_PATHWAY		MSigDB (19) (PID)
	PID_RAS_PATHWAY		MSigDB (19) (PID)
	WNT-PCP_PATHWAY		Compiled from Bottcher *et al.* 2021 (16) and Smith *et al.* 2020 (25)
E and Id protein target genes (**Figs. 2E, 3H, 5J-K**)	E2-2 (" TCF4_Q5" in the MSigDB)	E2-2 transcription factor target genes (Note: this is different from the WNT effector TCF4)	MSigDB (19)
	E47_01	E47 (splice isoform of E2A) transcription factor target genes	MSigDB (19)
	E47_02	E47 (splice isoform of E2A) transcription factor target genes	MSigDB (19)
	E12_Q6	E12 (splice isoform of E2A) transcription factor target genes	MSigDB (19)
	HEB_Q6	HEB transcription factor target genes	MSigDB (19)
	E2A_Q2	E2A transcription factor target genes	MSigDB (19)
	ID1_TARGETS (ID1_TARGET_GENES in the MSigDB)	Genes associated with upregulation of Id1	Kolmykov *et al.* 2020 (26); available in the MSigDB (19)
	ID2_TARGETS (ID2_TARGET_GENES in the MSigDB)	Genes associated with upregulation of Id2	Kolmykov *et al.* 2020 (26); available in the MSigDB (19)
Intestinal epithelial regeneration (**Figs. 5H-I, 6G-H**)	DSS-induced colitis regenerating epithelium	Genes enriched in regenerating colonic epithelium following DSS-induced injury	Wang *et al.* 2019 (27); derived from Yui *et al.* 2018 (28)
	Fetal epithelial gene signature	Genes enriched in fetal epithelial spheroids and "fetal-like reprogramming" of the regenerating intestinal epithelium	Wang *et al.* 2019 (27); derived from Mustata *et al.* 2013 (29) and Yui *et al.* 2018 (28)
	scRNA-seq cluster SSC2c "revival" cells	Genes enriched in sub-cluster SSC2c generated from unsupervised clustering of scRNA-seq generated from 12 Gy-irradiated and non-irradiated mouse intestinal epithelium. The SSC2c cluster, which appeared only after irradiation, was reported to contain quiescent "revival" stem cells induced by the YAP1 transcription factor.	Ayyaz *et al.* 2019 (30)

	Clu[+] "revival" cell signature	*Clu*-GFP^{+} cells FACS-sorted from irradiated *BAC-Clu*-GFP mice, described as a damage-induced "revival" stem cell population	Ayyaz *et al.* 2019 (30)
	Composite injury-regeneration signature	Gene set compiled from the above DSS-induced colitis regenerating epithelial, fetal epithelial, and "revival" cell signatures	Qu *et al.* 2021 (31)
	Ascl2[+] de-differentiating cell signature	Genes significantly upregulated in FACS-sorted, de-differentiating/regenerating *Ascl2*-mCh[+] "upper" cells from murine colon following diphtheria toxin (DT)-mediated ablation of Lgr5^{+} stem cells (compared to *Lgr5*^{+} stem cells FACS-sorted from uninjured *Lgr5*[Dtr-GFP] mouse colon)	Murata *et al.* 2020 (22)

62 **Table S3. Descriptions of gene sets used for GSEA.** Gene sets that are not available in the MSigDB are provided in Table S4.

Supplemental Figures
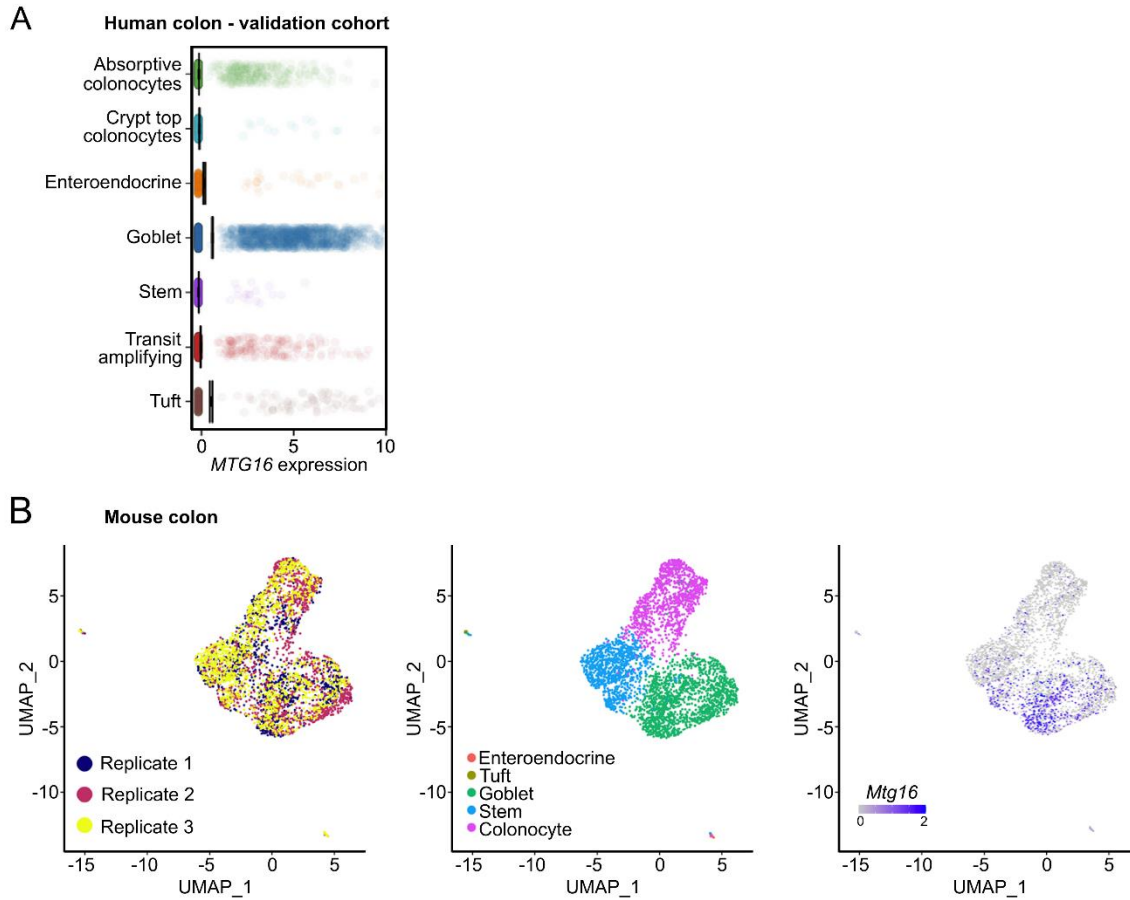
Figure S1. Extension of scRNA-seq data in Figure 1A-B. (A) *MTG16* expression in scRNA-seq of the human colon (validation cohort). 34,008 cells were sequenced from n = 31 normal human colon samples. **(B)** *Mtg16* expression in scRNA-seq of murine colonic epithelial isolates summarized by cell type in Figure 1B. Left, UMAP plot demonstrating n = 3 biological replicates. Middle, UMAP plot annotated by cell type. Right, UMAP plot demonstrating *Mtg16* expression in individual cells. 3,653 cells were sequenced.
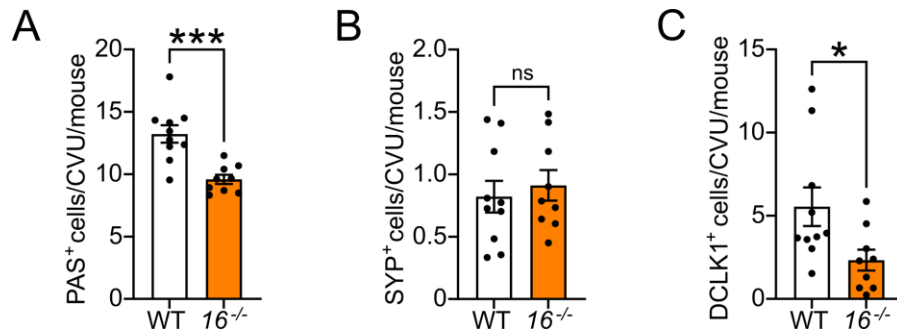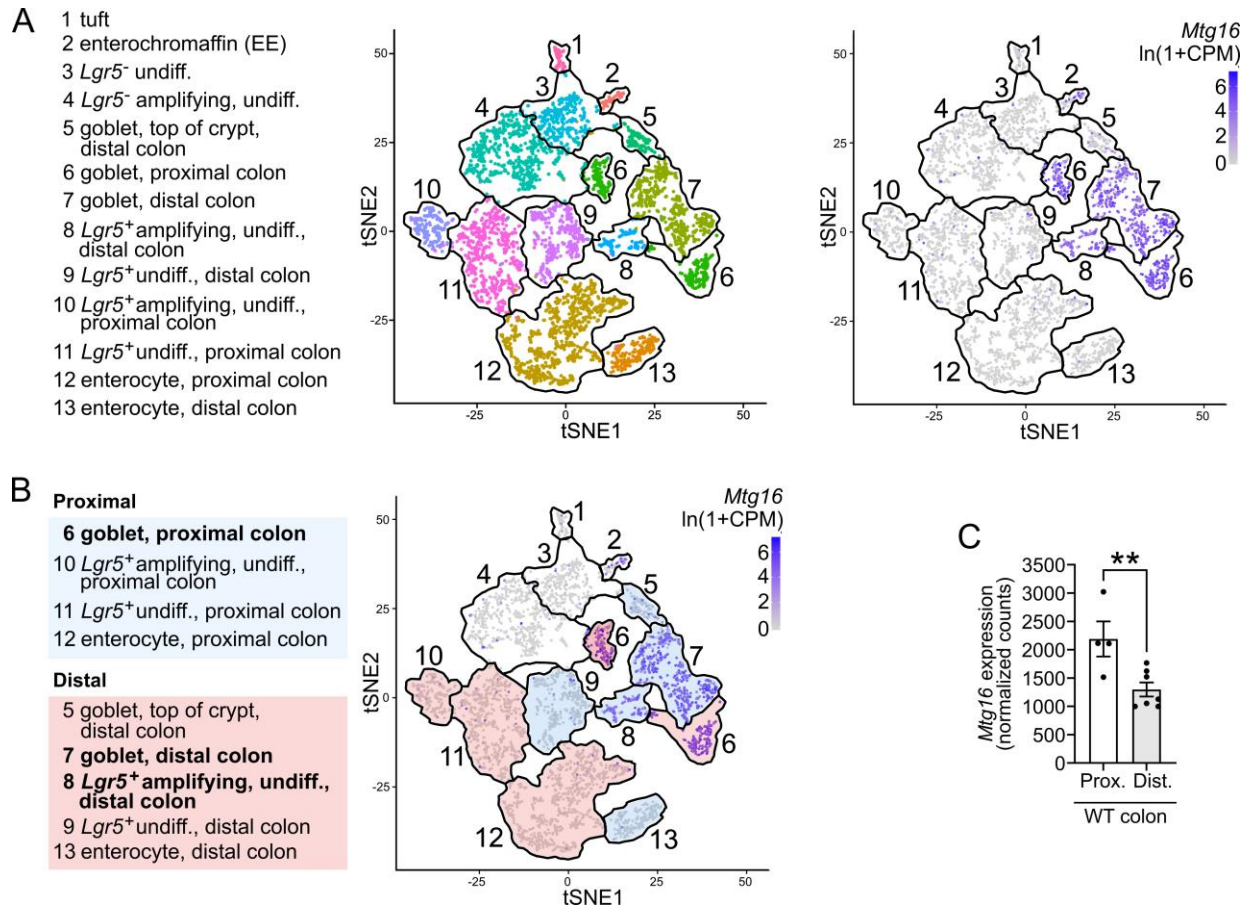
Figure S2. Secretory cell frequencies in the *Mtg16^{-/-}* SI. Quantification of **(A)** goblet cells per crypt-villus unit (CVU) by periodic acid-Schiff (PAS) stain, **(B)** enteroendocrine cells by IHC for synaptophysin (SYP), and **(C)** tuft cells by IHC for doublecortin-like kinase 1 (DCLK1) in WT and *Mtg16^{-/-}* small intestine (n = 10 WT, 9 *Mtg16^{-/-}*). *$p < 0.05$, ***$p < 0.001$ by two-tailed Mann-Whitney test.
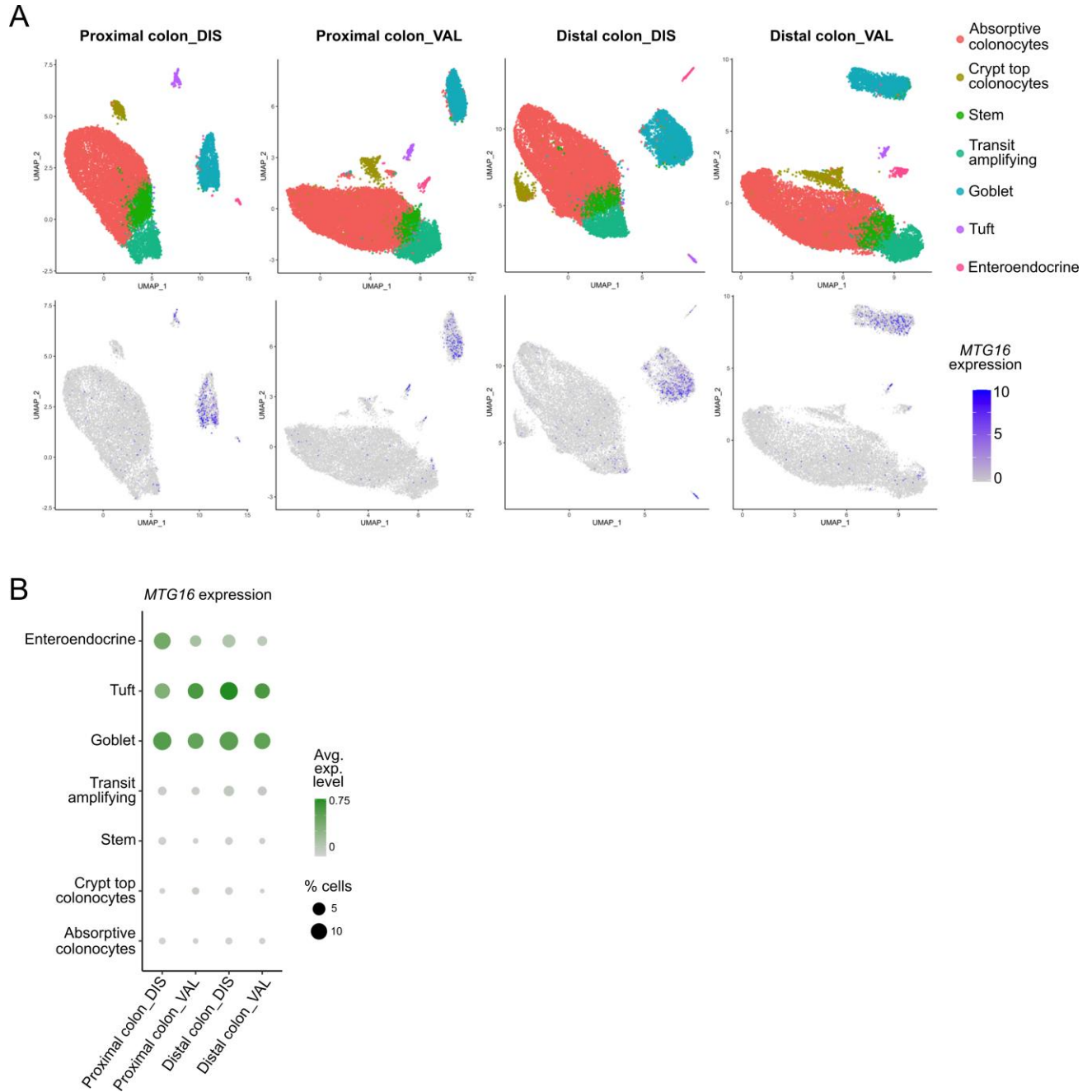
Figure S3. Differences between the proximal and distal human colon. (A) Annotated
colonic epithelial clusters (top) and corresponding *MTG16* expression (bottom) in human
proximal and distal normal colon biopsies queried from our scRNA-seq discovery (DIS) (n =
12,596 cells sequenced from 18 proximal colon samples and 17,778 cells sequenced from 17
distal colon samples) and validation (VAL) (n = 17,289 cells sequenced from 17 proximal colon
samples and 16,719 cells sequenced from 14 distal colon samples) cohorts. **(B)** *MTG16*
expression in the proximal and distal colon of each human cohort. Color gradient represents the
average *MTG16* expression level in each cell population. Dot size represents the percentage of cells
in each population expressing *MTG16.*

13

A
1 tuft
2 enterochromaffin (EE)
3 *Lgr5*⁻ undiff.
4 *Lgr5*⁻ amplifying, undiff.
5 goblet, top of crypt, distal colon
6 goblet, proximal colon
7 goblet, distal colon
8 *Lgr5*⁺amplifying, undiff., distal colon
9 *Lgr5*⁺undiff., distal colon
10 *Lgr5*⁺amplifying, undiff., proximal colon
11 *Lgr5*⁺undiff., proximal colon
12 enterocyte, proximal colon
13 enterocyte, distal colon

B
Proximal
6 goblet, proximal colon
10 *Lgr5*⁺amplifying, undiff., proximal colon
11 *Lgr5*⁺undiff., proximal colon
12 enterocyte, proximal colon

Distal
5 goblet, top of crypt, distal colon
7 goblet, distal colon
8 *Lgr5*⁺ amplifying, undiff., distal colon
9 *Lgr5*⁺undiff., distal colon
13 enterocyte, distal colon

87

Figure S4. Differences between the proximal and distal mouse colon. (A) Annotated colonic epithelial clusters (left) and corresponding *Mtg16* expression (right) queried from scRNA-seq of WT mouse colon (n = 6) publicly available in the *Tabula Muris* (8). **(B)** Alternate annotation emphasizing clusters representing cells specifically from the proximal (blue) or distal (red) colon. Bolded clusters denote clusters expressing *Mtg16*. **(C)** *Mtg16* expression (transcript counts normalized by DESeq2) in WT proximal and distal colon epithelial isolates (n = 4 proximal, 7 distal). **p_{adj} < 0.01 by DESeq2.
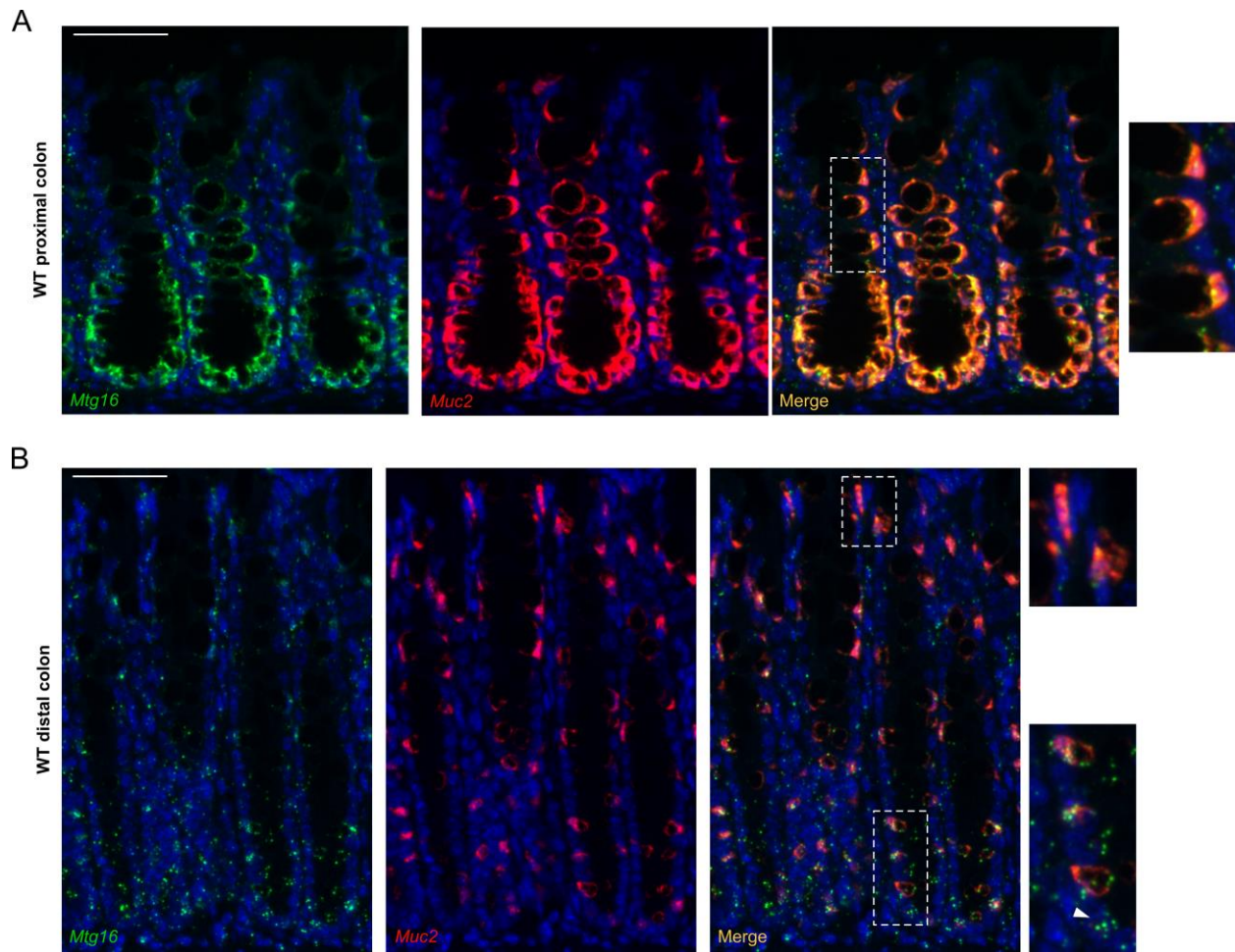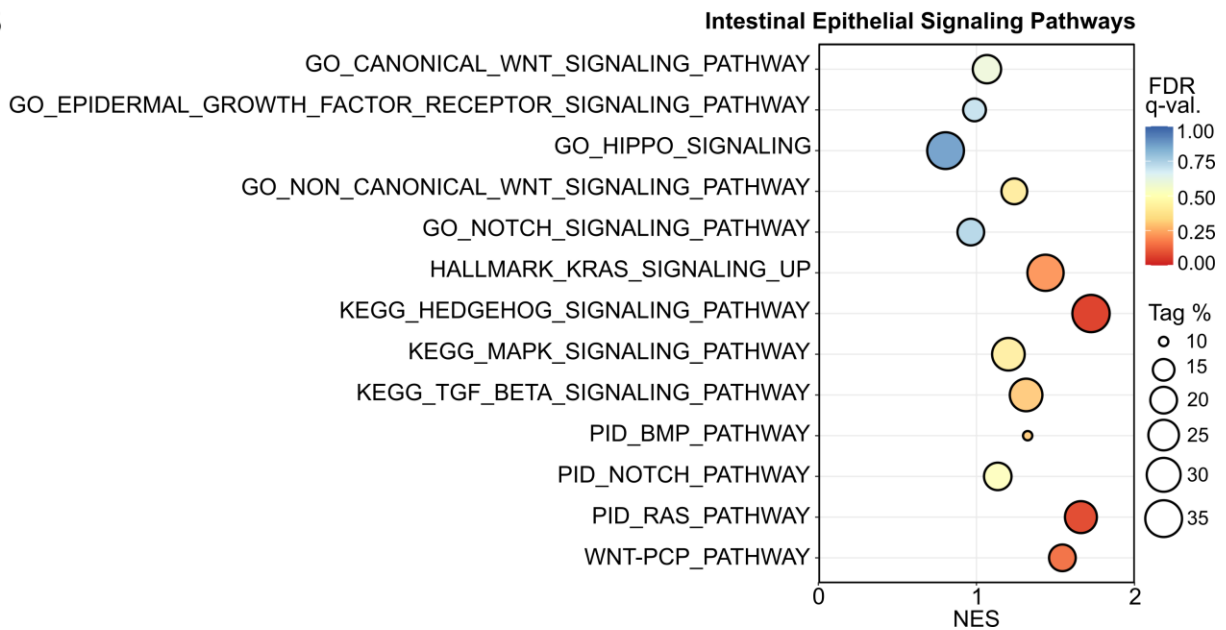
Figure S5. RNAscope *in situ* hybridization of *Mtg16* and *Muc2* indicating differential expression and co-localization of mRNA expression in WT mouse proximal (A) and distal (B) colon. Scale bars = 50 µm. White dashed lines denote insets at right. White arrow in **(B)** denotes an epithelial cell near the crypt base expressing *Mtg16*, but not *Muc2*.

A

B


100
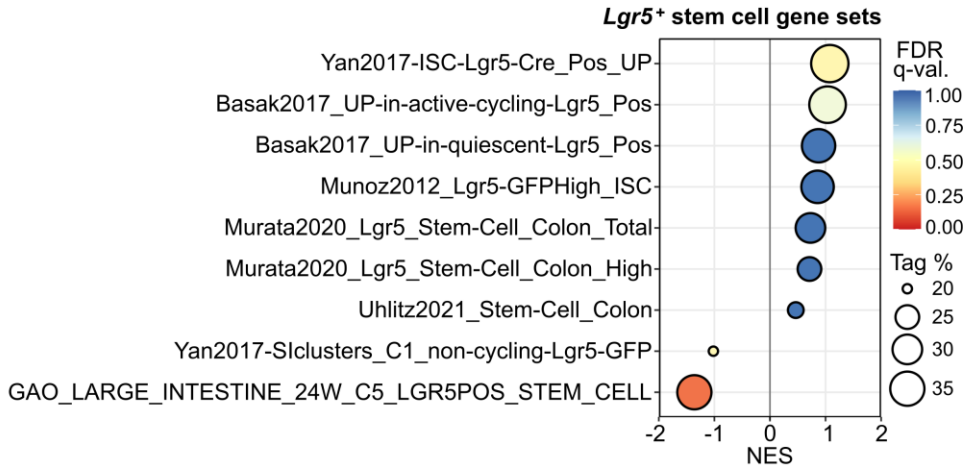
Figure S6. GSEA of stem cell and signaling pathway gene sets in the *Mtg16$^{-/-}$* distal colon.
GSEA of distal colon RNA-seq (n = 4 WT, 4 *Mtg16$^{-/-}$*) using **(A)** multiple gene sets representing
Lgr5$^+$ stem cells derived from the literature and **(B)** gene sets for intestinal epithelial signaling
pathways (described in Tables S3 and S4). NES, normalized enrichment score (ES). Tag % is
defined as the percentage of gene hits before (for positive ES) or after (for negative ES) the
peak in the running ES, indicating the percentage of genes contributing to the ES. FDR q-value
< 0.05 is considered significant.

108

109
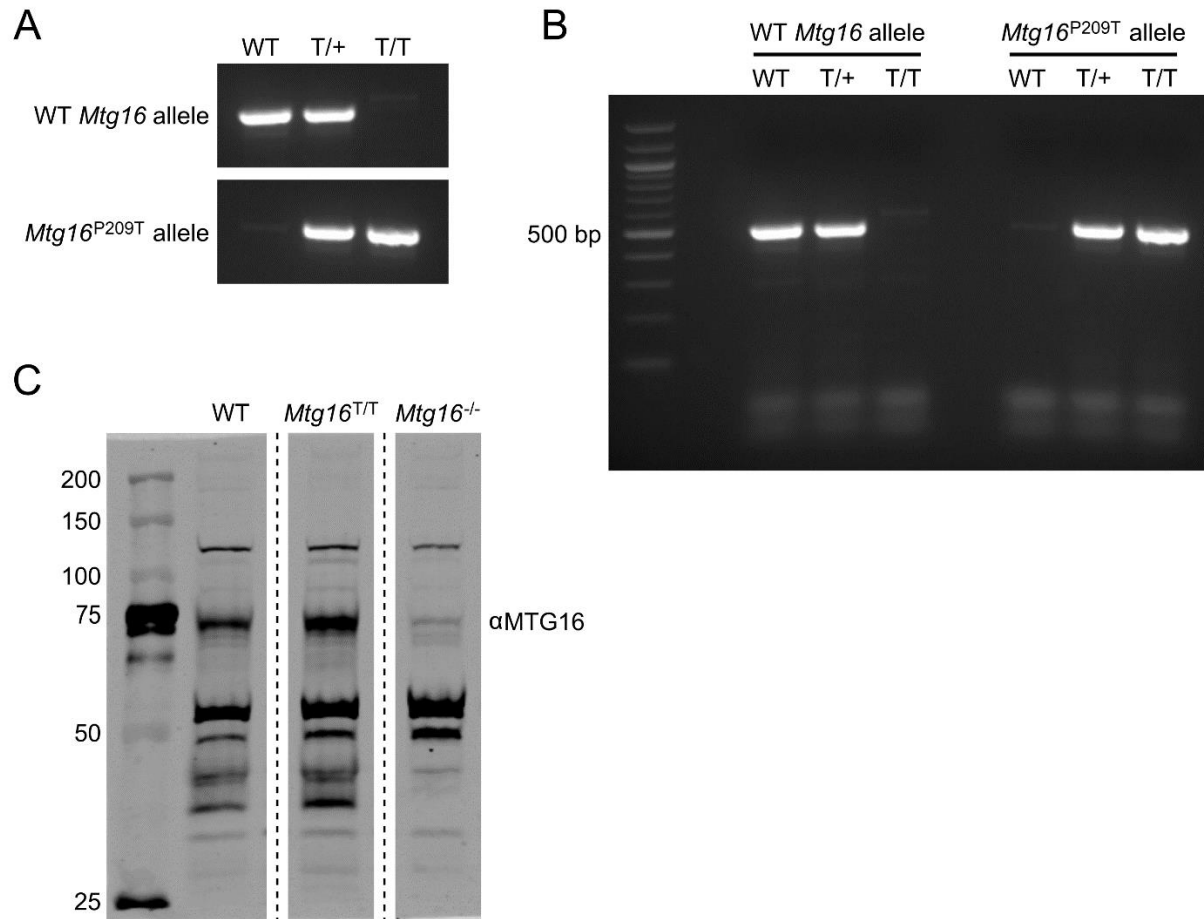
Figure S7. Validation of the _Mtg16_^{P209T} mouse model. (A-B) Representative PCR reactions
for WT _Mtg16_ and _Mtg16_^{P209T} alleles on WT, heterozygous _Mtg16_^{P209T} mutant (_Mtg16_^{T/T}), and
homozygous _Mtg16_^{P209T} mutant (_Mtg16_^{T/T}) mice. **(A)** PCR for the WT _Mtg16_ allele performed
using the primers SWH1432 and SWH1438 (top) and PCR for the _Mtg16_^{P209T} mutant allele
performed using primers SWH1432 and SWH1435 (bottom). **(B)** Uncropped image of 2%
agarose gel used to generate **(A)**, demonstrating the expected length of PCR products using a
100 bp DNA ladder (#B7025, New England Biolabs). **(C)** Immunoblot (lanes spliced from the
same membrane imaged under the same conditions) demonstrating MTG16^{P209T} expression at
the expected molecular weight in bone marrow lysates from _Mtg16_^{T/T} mice, compared to WT
(positive control) and _Mtg16_^{-/-} (negative control).
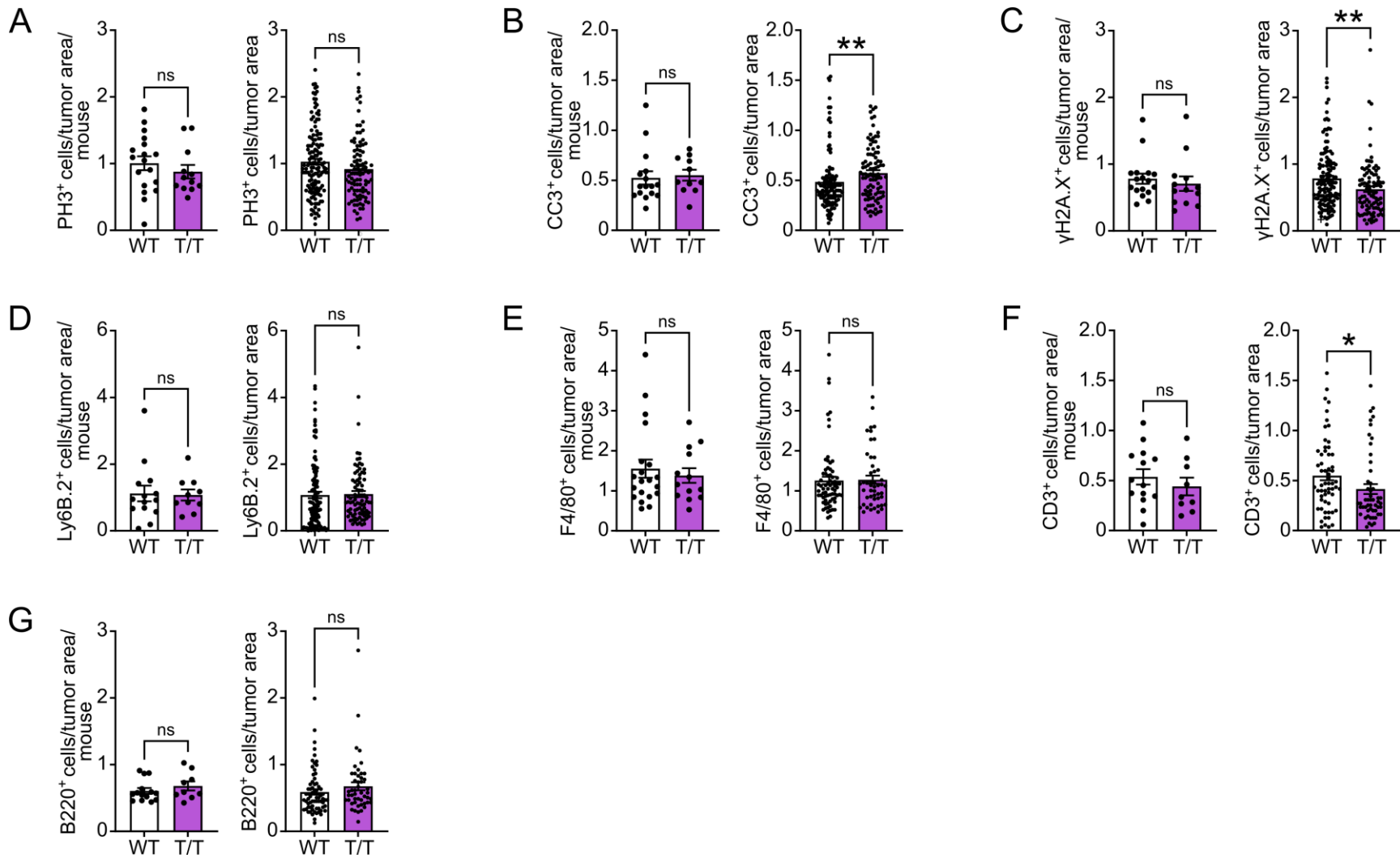
Figure S8. Additional characterization of AOM/DSS tumors by immunofluorescent staining. Characterization of tumor epithelial cells by quantification of **(A)** phospho-histone H3-positive (PH3+) proliferating cells, **(B)** cleaved caspase-3-positive (CC3+) cells undergoing apoptosis, and **(C)** γH2A.X+ cells (nuclei) displaying DNA damage. Quantification of intratumoral **(D)** Ly6B.2+ neutrophils, **(E)** F4/80+ macrophages, **(F)** CD3+ T cells, and **(G)** B220+ B cells. **(A-G)** Left, quantification and analysis by average number of cells

125   per tumor area (10^6 pixels) per mouse (n = 9-18 mice). Right, quantification analyzed by tumor area (n = 48-137). *$p < 0.05$, **$p <$
126   0.01 by two-tailed Mann-Whitney test.
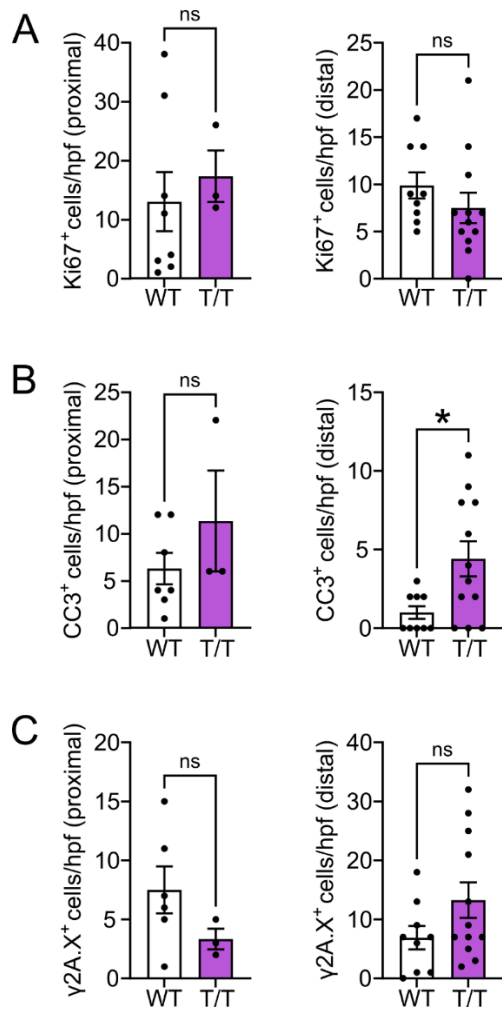
Figure S9. Characterization of tumoroids derived from proximal (left) and distal (right) AOM/DSS tumors by immunofluorescent staining. Quantification of **(A)** Ki67+ proliferating cells, **(B)** cleaved caspase-3-positive (CC3+) cells undergoing apoptosis, and **(C)** yH2A.X+ cells (nuclei) displaying DNA damage per high-power field (hpf). n = 3-12 hpf from 1-4 tumoroid lines. *$p < 0.05$ by two-tailed Mann-Whitney test.

Supplemental References

1. Rajamäki K et al. Genetic and epigenetic characteristics of inflammatory bowel disease associated colorectal cancer. *Gastroenterology* [published online ahead of print: 2021]; doi:10.1053/j.gastro.2021.04.042

2. Patro R, Duggal G, Love MI, Irizarry RA, Kingsford C. Salmon: fast and bias-aware quantification of transcript expression using dual-phase inference. *Nat Methods* 2017;14(4):417–419.

3. Love MI, Huber W, Anders S. Moderated estimation of fold change and dispersion for RNA-seq data with DESeq2. *Genome Biol* 2014;15(12):550.

4. Ritchie ME et al. limma powers differential expression analyses for RNA-sequencing and microarray studies. *Nucleic Acids Res* 2015;43(7):e47–e47.

5. Thompson JJ et al. Blood vessel epicardial substance reduces LRP6 receptor and cytoplasmic β-catenin levels to modulate Wnt signaling and intestinal homeostasis. *Carcinogenesis* 2019;40(9):1086–1098.

6. Amend SR, Valkenburg KC, Pienta KJ. Murine Hind Limb Long Bone Dissection and Bone Marrow Isolation. *J Vis Exp Jove* 2016;(110):53936.

7. Thorvaldsdóttir H, Robinson JT, Mesirov JP. Integrative Genomics Viewer (IGV): high-performance genomics data visualization and exploration. *Brief Bioinform* 2013;14(2):178–192.

8. Schaum N et al. Single-cell transcriptomics of 20 mouse organs creates a Tabula Muris. *Nature* 2018;562(7727):367–372.

9. Dieleman et al. Chronic experimental colitis induced by dextran sulphate sodium (DSS) is characterized by Th1 and Th2 cytokines. *Clin Exp Immunol* 1998;114(3):385–391.

10. Fukata M et al. Toll-like receptor-4 promotes the development of colitis-associated colorectal tumors.. *Gastroenterology* 2007;133(6):1869--81.

11. Haber AL et al. A single-cell survey of the small intestinal epithelium. *Nature* 2017;551(7680):333–339.

12. Parikh K et al. Colonic epithelial cell diversity in health and inflammatory bowel disease. *Nature* 2019;567(7746):49–55.

13. Gehart H et al. Identification of Enteroendocrine Regulators by Real-Time Single-Cell Differentiation Mapping. *Cell* 2019;176(5):1158-1173.e16.

14. Li HJ, Ray SK, Kucukural A, Gradwohl G, Leiter AB. Reduced Neurog3 Gene Dosage Shifts Enteroendocrine Progenitor Towards Goblet Cell Lineage in the Mouse Intestine. *Cell Mol Gastroenterology Hepatology* [published online ahead of print: 2020]; doi:10.1016/j.jcmgh.2020.08.006

167   15. Yan KS et al. Intestinal Enteroendocrine Lineage Cells Possess Homeostatic and Injury-
168   Inducible Stem Cell Activity. *Cell Stem Cell* 2017;21(1):78-90.e6.

169   16. Böttcher A et al. Non-canonical Wnt/PCP signalling regulates intestinal stem cell lineage
170   priming towards enteroendocrine and Paneth cell fates. *Nat Cell Biol* 2021;23(1):23–31.

171   17. Kim T-H et al. Broadly permissive intestinal chromatin underlies lateral inhibition and cell
172   plasticity.. *Nature* 2014;506(7489):511 515.

173   18. Gao S et al. Tracing the temporal-spatial transcriptome landscapes of the human fetal
174   digestive tract using single-cell RNA-sequencing. *Nat Cell Biol* 2018;20(6):721–734.

175   19. Liberzon A et al. Molecular signatures database (MSigDB) 3.0. *Bioinformatics*
176   2011;27(12):1739–1740.

177   20. Powell AE et al. The Pan-ErbB Negative Regulator Lrig1 Is an Intestinal Stem Cell Marker
178   that Functions as a Tumor Suppressor. *Cell* 2012;149(1):146–158.

179   21. Muñoz J et al. The Lgr5 intestinal stem cell signature: robust expression of proposed
180   quiescent '+4' cell markers. *Embo J* 2012;31(14):3079–3091.

181   22. Murata K et al. Ascl2-Dependent Cell Dedifferentiation Drives Regeneration of Ablated
182   Intestinal Stem Cells. *Cell Stem Cell* 2020;26(3):377-390.e6.

183   23. Basak O et al. Induced Quiescence of Lgr5+ Stem Cells in Intestinal Organoids Enables
184   Differentiation of Hormone-Producing Enteroendocrine Cells. *Cell Stem Cell* 2017;20(2):177-
185   190.e4.

186   24. Basak O et al. Mapping early fate determination in Lgr5+ crypt stem cells using a novel
187   Ki67-RFP allele. *Embo J* 2014;33(18):2057–2068.

188   25. Smith JR et al. The Year of the Rat: The Rat Genome Database at 20: a multi-species
189   knowledgebase and analysis platform. *Nucleic Acids Res* 2019;48(D1):D731–D742.

190   26. Kolmykov S et al. GTRD: an integrated view of transcription regulation. *Nucleic Acids Res*
191   2020;49(D1):gkaa1057-.

192   27. Wang Y et al. Long-Term Culture Captures Injury-Repair Cycles of Colonic Stem Cells. *Cell*
193   2019;179(5):1144-1159.e15.

194   28. Yui S et al. YAP/TAZ-Dependent Reprogramming of Colonic Epithelium Links ECM
195   Remodeling to Tissue Regeneration. *Cell Stem Cell* 2018;22(1):35-49.e7.

196   29. Mustata RC et al. Identification of Lgr5-Independent Spheroid-Generating Progenitors of the
197   Mouse Fetal Intestinal Epithelium. *Cell Reports* 2013;5(2):421–432.

198   30. Ayyaz A et al. Single-cell transcriptomes of the regenerating intestine reveal a revival stem
199   cell.. *Nature* 2019;569(7754):121–125.

200   31. Qu M et al. Establishment of intestinal organoid cultures modeling injury-associated
201   epithelial regeneration. *Cell Res* 2021;1–13.

Fully uncropped agarose gel used to make Figure S7A-B. Areas surrounded by red rectangles were used in A.

The same fully uncropped agarose gel used to make Figure S7A-B. Area surrounded by red rectangle (all lanes) were used in B.
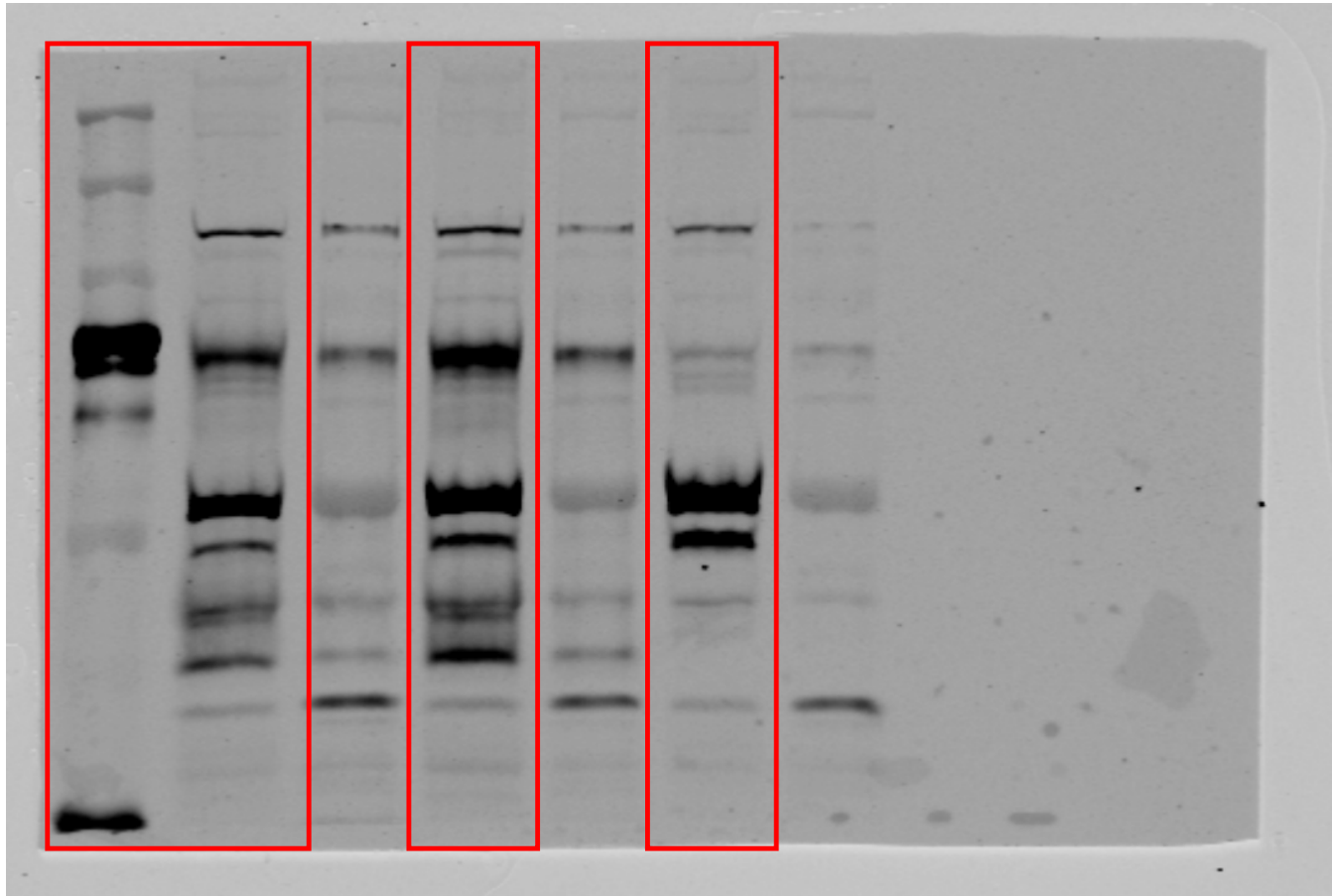
Uncropped immunoblot used to generate Figure S7C. The areas that were spliced together for the figure are surrounded with red rectangles.